Fully-Passive Wireless Implant for Neuropotential Acquisition: An *In Vivo* Validation

Carolina Moncion, Student Member, IEEE, Lakshmini Balachandar, Satheesh Bojja Venkatakrishnan, Student Member, IEEE, Jorge J. Riera, Member, IEEE, and John L. Volakis Fellow, IEEE

Abstract Implantable systems are often employed to perform continuous high-resolution recordings of neural activity. These systems frequently require invasive procedures when implanting and maintaining effective operation. This causes major interruptions to daily life. Previous work demonstrated an *in vitro* minimum detectable signal (MDS) of 15 μV in amplitude and RF sensitivity down to - 135 dBm. This suggests the possibility of detecting diminutive biopotentials in a wireless fully-passive manner. Here, for the first time, we validate this system through a series of *in vivo* electrophysiological recordings including both spontaneous cardiac activity and sensory evoked neural activity, with amplitudes ranging from a few microvolts to millivolts and across a spectrum of frequencies. We also present design considerations and the development of probes for neurosensing to accomplish detectability of biopotentials in the tens of microvolts in rats. The developed probes show improved impedance matching with the neurosensing system. Specifically, the new probes showed an impedance several orders of magnitude lower than those commercially available, thereby significantly improving signal detection. Notably, the presented *in vivo* validation of this technology has great future clinical implications in neuroscience as it offers a wireless and unobtrusive device for neurological research, monitoring, and therapeutic purposes.

Keywords - Biomedical Telemetry, Brain implant, Electroencephalography, Impedance Matching, Neuroscience

I. INTRODUCTION

The medical field is becoming increasingly dependent on wearable biotelemetry devices attached to the human body to monitor physiological parameters [1]. As of 2012, statistics show that about 27% of individuals use a wearable device, with this figure continuing to rise [2]. Neural activation monitoring is one of the applications of highest significance for these devices. To obtain these biological electroencephalogram (EEG) is typically used, resulting in the scalp-level recording of neural activation across an area of the cerebral cortex [3]. This EEG signal is recorded superficially, therefore sensing is limited to the cortex and is attenuated by the protective layers of the brain namely scalp, skull, meninges, etc., making recording a challenge [3]–[5].

To improve signal quality and achievable spatial resolution, electrocorticograms (ECoG) are often adopted [3]. For ECoG, the electrodes are placed on the cortical surface thereby omitting the signal attenuation issues of EEG [3], [5]. Notably, neural activation can have amplitudes from microvolts to the millivolts scale with frequencies ranging from 1 Hz to several hundred hertz or kilohertz, depending on the type of signal recorded (i.e. local field potentials, spikes, action potentials etc.) [1], [3], [6]–[8].

This paper is an expanded paper from IEEE IMBioC 2018, Philadelphia, PA. This work was supported by the U.S. National Science Foundation (NSF) under Award Number 1763350.

Carolina Moncion is with the NMD Laboratory and the RFCOM Laboratory at Florida International University Engineering Center, Miami, FL 33174 USA. (email: cmonc007@fiu.edu)

Lakshmini Balachandar (email: lbala010@fu.edu) and Jorge J. Riera (email: jrieradi@fu.edu) are with the NMD Laboratory at Florida International University Engineering Center, Miami, FL 33174 USA.

Satheesh Bojja-Venkatakrishnan (email: sbojjave@fiu.edu) and John L. Volakis (email: jvolakis@fiu.edu) are with the RFCOM Laboratory at Florida International University Engineering Center. Miami. FL 33174 USA

While ECoG is a better approach for signal recording it is highly invasive and this creates challenges in maintaining proper system functioning. Notably, current ECoG technology requires wires or connectors that are left protruding from the patient's head [9]. This affects quality-of-life and also alters the recording environment [5]. Implanted sensors have been introduced to avoid wire protrusions. However, these implants require a power source implying heat generation that can damage the neural tissues. By IEEE standards the maximum temperature increase should not exceed 1 °C from normal [1], [6], [10]. Of equal concern is the need to replace the batteries used to power the implanted circuits. Recent implants, no longer use batteries, but their demonstration has only been done *in vitro* [11].

Expanding on previous work, for the first time, we present the *in vivo* validation of the wireless and fully-passive implant in [11]. An essential step in this accomplishment was the development of electrodes or probes whose impedance is more suited for matching to the implant circuitry. For this reason, we begin with a description of the parameters considered, followed by an equivalent circuit model-based simulation and impedance measurements of three prototype probes. Testing of the probes with the wireless system was performed in two parts: 1) in vitro in a medium simulating the brain and 2) in vivo, for recording a large biopotential (cardiac signal) and for the most substantial result, using an induced neural signal.

II. WIRELESS NEUROSENSING SYSTEM

As portrayed in Fig. 1, the key components of our wireless and batteryless wireless neurosensing system (WiNS) are a) the implant and interrogator, b) probes, and c) demodulation circuit. The recorder was designed such that the implant could be placed beneath the scalp using a small incision. The implant

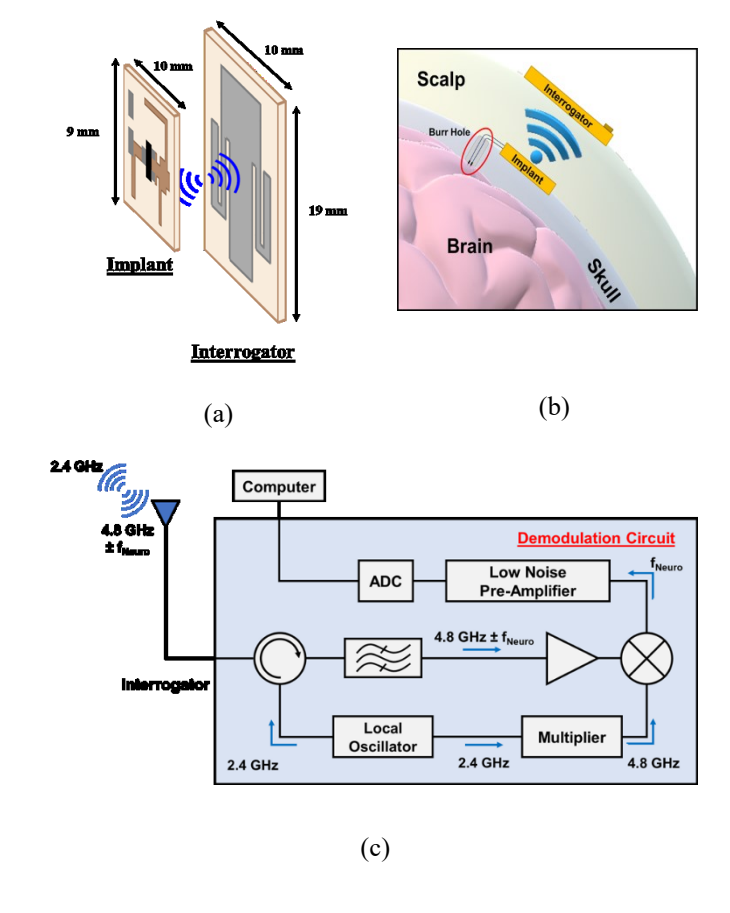


Fig. 1. WiNS and major components (a) dimensions of implant and interrogator, with the anti-parallel diode pair (APDP) highlighted (b) schematic of system implementation with probe positioning highlighted (c) simplified version of demodulation circuit with connection to interrogator and computer.

connects to the surface of the cerebral cortex via the probes that are surgically inserted through a burr hole. As highlighted in Fig. 1 the implant communicates wirelessly with the exterior interrogator, which is in turn connected to the demodulation circuit for filtering, amplification, and extraction of the neural signal.

A. Implant and Interrogator

Both the implant and interrogator are equipped with highly efficient dual-band antennas devised to radiate at 2.4 and 4.8 GHz \pm f_{neuro} and achieve good EM coupling in the near field [11], [12]. As shown in Fig. 1(a), the implant has dimensions of 10 mm x 9 mm, while the interrogator has a slightly larger footprint at 10 mm x 19 mm. For sensing, a 2.4 GHz signal is transmitted to the implant using the external interrogator. This carrier signal provides the necessary turn-on voltage for the implanted antiparallel diode pair (APDP), circled in Fig. 1, where it is harmonically mixed with the neural signal [11], [12]. The APDP performs this efficiently, as both the negative and positive component of the carrier signal is captured [12]. The output of the mixer is 4.8 GHz \pm f_{neuro}, this is backscattered to the interrogator [11], [12].

The major unique feature of this WiNS is its fully-passive functionality. This is due to its simple electronics, mainly the previously mentioned APDP [11]. Herewith, the term fullypassive refers to a system or device without internal energy source [6]. We note that the APDP in this implant is simply triggered by the carrier signal and the signal is not used as a formal energy source. This not only addresses the issue of heat generation caused by power dissipation but also reduces the likelihood of revision procedures associated with internal batteries. To further ensure its unobtrusiveness and biocompatibility, the implant was encapsulated in a PDMS layer (implant thickness including layer is about 3 mm) which isolates its metallization from biological tissues [11], [13]. In addition to contributing to the biocompatibility of the system, the PDMS layer also serves to improve the implanted antenna's efficiency by increasing the transmission coefficient between the antennas [12], [14]

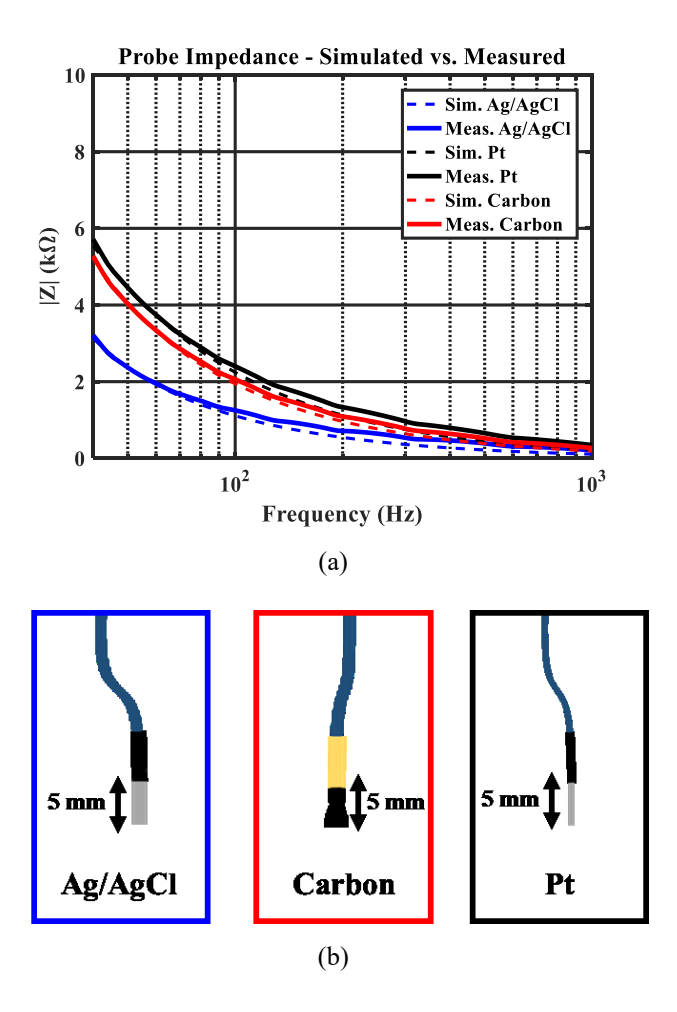


Fig. 2. Prototype probes developed in-house. (a) Simulated and measured results of probe impedance characterization, the simulated results were obtained using an equivalent circuit model of each probe. (b) Schematic of each of the probes. Ag/AgCl: Silver-Silver Chloride, Pt: Platinum

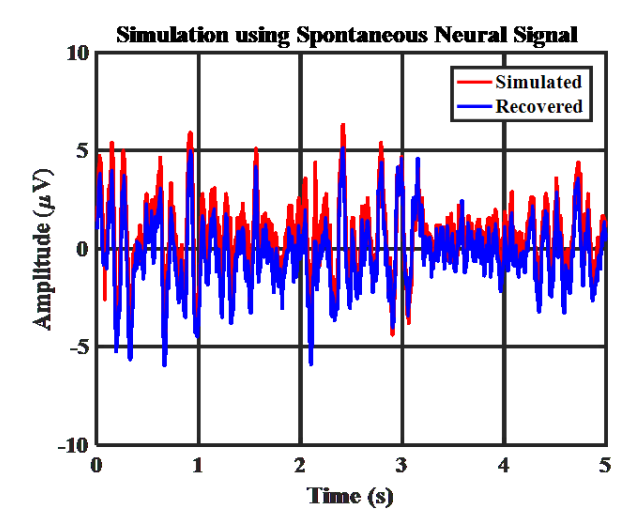


Fig. 3. Overlay of simulated and recovered neural signal from *in vitro* experiment used to evaluated WiNS sensing abilities. The simulated and recovered signal have a significant correlation coefficient of 0.9521 ($\alpha = 0.05$).

B. Probes

The developed WiNS implant has an input impedance of approximately 50Ω . However, available commercial probes have impedances on the order of $M\Omega$ to closely match the input impedance of typical devices [4], [7]. It is, therefore, necessary to develop low-impedance probes, for better matching a 50Ω impedance. To do so, we must consider several properties that affect probe impedance, including geometry, material selection and surface area [15]. These properties were tested and confirmed, here we present the results for the silver-silver chloride (Ag/AgCl), carbon and platinum (Pt) probes.

To start, we set constraints to the dimensions of the probes (no larger than 5 mm in length and 0.5 mm in radius) to ensure a minuscule footprint, then based on available material properties we constructed an equivalent circuit model for each probe consideration and simulated the impedance magnitude over a range of frequencies. Prototypes of each of the probes were developed in our lab starting with either silver, platinum or carbon wire. To fabricate the Ag/AgCl probes, a silver wire was purchased and electrochemically coated with chloride. The appropriate process was repeated for the carbon and Pt probes. Afterward, each probe was characterized, using a precision impedance analyzer (Keysight 4292A). Fig. 2 (a) shows a close match between the simulated and measured impedance values of the three prototypes shown schematically in Fig. 2 (b) and an overall impedance in the order of $k\Omega$. Fig. 2 (b) includes the approximate length of each probe, kept uniform for each prototype, the corresponding radii are 0.5 mm, 0.5 mm and 0.15 mm for Ag/AgCl, carbon and Pt, respectively. These prototypes were then used for in vitro and in vivo evaluation.

The impedance of all three probes is shown in Fig. 2. We note that the Ag/AgCl and carbon probes have the lower impedance, especially the Ag/AgCl probes have an impedance which is about 1 k Ω as compared to the M Ω values of the commercially-available probes. These probes were also minimally invasive, thus achieving the required characteristics to appropriately sense different biopotentials.

C. Demodulation Circuit

The demodulation circuit serves to extract the neural signal from the modulated signal centered at 4.8 GHz, in other words it is used for down conversion. To analyze the modulated signal, a spectrum analyzer can be used as a display, however clinically relevant components are better visualized in the timedomain. For this reason, here we only present the demodulated signal in the time domain and exclude the spectrum analyzer from Fig. 1(c). As depicted in Fig. 1(c), the modulated 4.8 GHz ± f_{neuro} goes through filtering and amplification before being demodulated in the mixer, followed by another amplification before being digitized and stored. Fig. 1 (c), is a representation of the circuit, in reality it is composed of several filtering and amplification stages before demodulation, however, we note that the circuit has very low reported noise figure of 3.8 dB [11]. A detailed description of the demodulation circuit used herewith, inleuding part specifications, can be found in [11].

III. METHODS AND PROCEDURES

A. In Vitro Experiment

An experimental set up was designed to test the WiNS prior to the *in vivo* scenario. In this setup, an authentic neural activation signal, corresponding to a previously recorded alpha rhythm, was emulated and sensed using the proposed WiNS. This signal was a segment of an EEG recording performed on a healthy subject as part of an Institutional Review Board (IRB) at Florida International University approved study (Approval

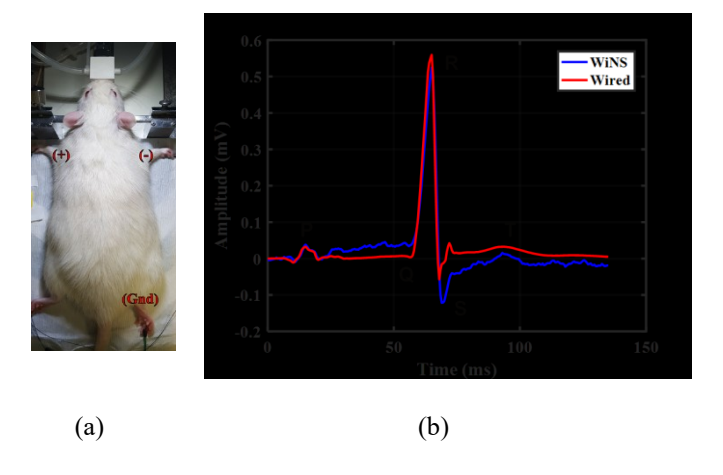


Fig. 4. Cardiac activity recording. (a) Representation of probe placement in a ECG Lead-I configuration on Wistar rat. (b) Overlay of average WiNS and wired ECG waveform recorded using the developed Ag/AgCl probes, these waveforms have a significant correlation coefficient of 0.9306 (α = 0.05).

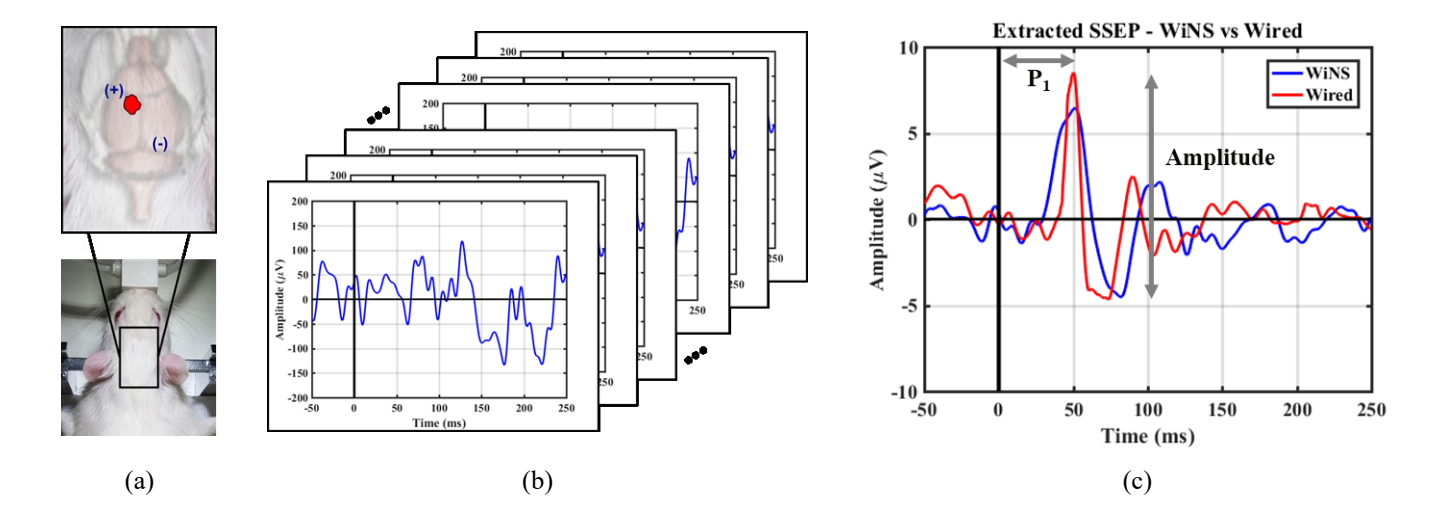


Fig. 5. Neural activity recording. (a) Schematic of area of interest (primary somatosensory cortex, hind limb region contralateral to the stimulated hindpaw) and probe placement during recording. (b) Representation of signal averaging procedure used during the signal processing stage of neural recording. (c) Overlay of WiNS and wired extracted somatosensory evoked potential (SSEP) after processing the signal.

No. 17-0072). Human neural activity can be classified into several brain waves: alpha, beta, and gamma [8]. The major frequency components of alpha rhythms typically range between 8-12 Hz and they emanate from the visual cortex of the brain [8].

Previously, our neurosensor was tested using a single tone sinusoidal signal. While this waveform can be used to represent a neural signal, a multifrequency signal like the previously described alpha rhythm recording provides a more realistic setup. In addition, during this experiment rather than supplying the emulated signal directly to the WiNS implant, the signal was induced in a normal (0.9%) saline solution to represent the conductive properties of the brain and its interaction with the neural probes. Furthermore, to emulate the medium between the implant and interrogator a substitute phantom material was used [11], [12]. During this experiment, WiNS was set up analogous to Fig. 1 (b), the carrier signal power level supplied to the interrogator for transmission was kept at 6 dBm, in accordance with the power level determined in [11], to meet the requirements for receiving the backscattered signal and those of FCC and ICNIRP for subject safety. In this paper, for the first time, the implant and interrogator will be evaluated in an actual animal experiment.

B. Animal Preparation

All experimental procedures were approved by and carried out in compliance with the Institutional Animal Care and Use Committee (IACUC) at Florida International University (Approval No. 17-042). Wistar rats (Charles River Laboratories, Wilmington, MA) were housed in standard cages at a 12h-12h light-dark cycle with free access to food and water. They were given at least one week of acclimation before initiating either of the biopotential recordings.

The rats were anesthetized with isoflurane (5% for initial induction, 1.5-2.5%, 1 L/min O₂, 14.7 PSI) throughout any manipulation, including fixing in a stereotaxy (Narishige, Japan) and probe insertion. During the neural recording, the rats were anesthetized with a mixture of dexmedetomidine hydrochloride (Dexdomitor, 0.25 mg/kg, i.p.) and low doses of isoflurane (0.5%, 1L/min O₂, 14.7 PSI). Body temperature was maintained with a heating pad (TPZ-0510EA, Texas Scientific Instruments, LLC) and a pump (TP700, Texas Scientific Instruments, LLC) at about 36°C. Respiration rate was sustained between 55-60 breaths per minute. Temperature and breathing were both monitored throughout the procedure using AD Instruments PowerLab 8/35 data acquisition device and LabChart software to ensure stability.

C. Cardiac Activity Recording

Our initial experimental goal was to record electrocardiographic (ECG) signals. While evidently different from neural activity, this signal was selected as a proof-of-concept for WiNS, due to its large amplitude (in the millivolts scale). For the ECG measurements, the probes were placed in a common ECG-Lead I configuration. This set up is seen in Fig. 4(a) where the positive probe was placed on the left forelimb and the reference located on the right forelimb of the animal. Fig. 4(a) also includes a representation of the ground probe placement on the right hind limb.

Using the set up in Fig. 4(a), both the WiNS and wired recordings were carried out. The wired recordings were done using the AD Instruments Animal Bio Amp. The AD Instruments Powerlab 8/35 was used for saving both the WiNS and wired data at a sampling rate of 1 kHz. For WiNS, a signal generator was used to supply the required 2.4 GHz carrier signal to the interrogator at a 6 dBm power level. The actual recording was performed for 20 minutes. Filtering was not

required when processing the cardiac recording as the signal is greater in strength than the neural activity and therefore less susceptible to interference. The recordings were averaged to obtain a representative PQRST waveform (see Fig. 4(b)) for both systems.

D. Neural Activity Recording

As previously noted, neural signals do not exhibit a distinct waveform like ECG. Therefore, neural signals require extensive processing and analysis to extract applicable information. To address this, we implemented a stimulation paradigm and extracted somatosensory evoked potentials (SSEP) [7], [16]. The stimulation is analogous to that in [17]. Specifically, pulses (3 Hz, 2.5 mA, and 0.5 ms duration) were excited via the rat's hind paw using an isolated pulse stimulator (AM Systems Model 2100). Two small needle electrodes were inserted subcutaneously in the right hind paw to induce neural activity. The resulting activity at S1HL (primary somatosensory cortex, hind limb region) was recorded and processed. Fig. 5(a) portrays the approximate placement of the positive and reference probes. This location was identified using [18].

The AD Instruments PowerLab 8/35 data acquisition device was used to save the demodulated WiNS and wired neural signal. A trigger signal from the pulse stimulator was also recorded to time-lock the neural activity during processing. All three signals (WiNS, wired and trigger) were recorded at a sampling rate of 2 kHz. Processing the neural signal required a 60 Hz notch filter to remove powerline interference. The signal was then bandpass filtered from 1 - 125 Hz. The stop frequencies of this filter were selected to ensure that the expected evoked neuropotentials were captured. Each SSEP was extracted from approximately 1000 trials. The trials were segmented from -50 ms to 250 ms referenced the stimulus onset trigger recorded. The Matlab-based EEGLab software was used to average the neuropotentials. We note that to reduce losses between the implant and interrogator a phantom layer that emulates the skin dielectric properties at 2.4 GHz and 4.8 GHz [14], [19], [20].

TABLE I

COMPONENT DETECTION LATENCY - WINS VS. WIRED

	Component	Latency (ms)	
		WiNS	Wired
Cardiac Activity			
	P	15	15
	Q	56	57
	R	65	65
	S	69	68
	T	93	94
Neural Activity			
Ž	\mathbf{P}_{1}	51.5	50

IV. RESULTS

A. In Vitro Experiment

Fig. 3 shows an overlay of the simulated authentic signal and the recovered signal. The results of this experiment confirm the WiNS's ability to sense signals with a realistic bandwidth. Visual inspection of the overlay implies a significant correlation, however to quantify this we calculated the metric. This revealed a significant correlation coefficient between the simulated and recovered signal of 0.9521 at a 0.05 significance level. This high correlation coefficient speaks to the ability of WiNS to sense minute signals, harmonically mix them with a carrier signal, transmit and then demodulate with minimal signal distortion. In other words, WiNS can be reliably used for sensing neural signals while maintaining signal integrity.

B. Cardiac Activity

Fig. 4(b) shows an overlay of the average WiNS and wired ECG waveform obtained from ~350 heartbeats. The developed Ag/AgCl probes were used for this recording. From Fig. 4(b), it is evident that the essential ECG components are easily identifiable. More importantly, the two recordings show excellent agreement, quantifiable with the obtained significant correlation coefficient of 0.9306 at a 0.05 significance level. A precise detection of the amplitude and timing or temporal resolution are significant during the analysis of this data. From Table I it is noted that there is never a delay greater than 1 ms between the peak of each component. This is a minor, and clinically irrelevant difference.

C. Neural Activity

Fig. 5(b) illustrates a sample epoch extracted from the raw neural signal recorded with the WiNS. Fig. 5(c) depicts an overlay of the WiNS and wired extracted potentials obtained with the prototype carbon probes developed. We note that while the Ag/AgCl and carbon probes exhibited a reduced impedance (Fig. 2(b)), their geometry is slightly different. This makes them appropriate for different biopotential recordings.

Fig. 5(c) indicates that in both recordings the characteristic components of the SSEP are present. Namely, a reduction in amplitude prior to and at the stimulus onset, followed by a positive component (P₁), then a negative component and a return to a reduced amplitude. Close examination of this shows a high correlation between the WiNS and wired extracted evoked potential. The P₁ component is measured as the time to the positive peak from the stimulus onset. As noted in Table I the evoked potential in Fig. 5 (c) has a P₁ latency of 51.5 ms for the WiNS recording compared to 50 for the wired recording. The evoked potential amplitude (measured between P₁ and the negative component) was 11 µV and 12 µV for the WiNS and wired recording, respectively. The slight discrepancy between the recordings can be attributed to the small cortical area of interest. According to [21], left hemisphere S1HL has a reported average anatomical volume of 4.44 ± 1.14 mm³, this is approximately 2% of the left hemisphere cerebral cortex of the

rat. This made it impossible to simultaneously record with both systems.

V. CONCLUSION

For the first time, we presented the *in vivo* validation of a wireless fully-passive system. The developments that made it possible to expand on previous work [11] and realize this include.

- 1) probes with reduced impedance
- evoked potential paradigm to induce specific neural activity

The probes were designed to maximize signal transfer to the implant allowing us to demonstrate the successful recording of both cardiac and neural activity. On the other hand, the evoked potential paradigm was instrumental in sensing a verified neuropotential. These results imply that our neurosensor can detect the signals generated by the brain in a wireless fully-passive manner. As such, it is a revolutionary device with a broad spectrum of applications in neuroscience including epilepsy studies, in addition to, brain-computer interfacing (BCI) and brain-machine interfacing for prosthesis control.

ACKNOWLEDGMENT

The authors would like to thank Asimina Kiourti and Wei-Chuan Chen from the Electroscience Laboratory (ESL) at The Ohio State University for their guidance on implementing this system and research.

REFERENCES

- V. M. Bafar and A. Schmid, Wireless cortical implantable systems, vol. 9781461467, 2012.
- [2] A. Kiourti and K. S. Nikita, "A review of in-body biotelemetry devices: Implantables, ingestibles, and injectables," *IEEE Transactions on Biomedical Engineering*, vol. 64, no. 7. pp. 1422–1430, 2017.
- [3] G. Buzsáki, C. A. Anastassiou, and C. Koch, "The origin of extracellular fields and currents-EEG, ECoG, LFP and spikes," *Nat. Rev. Neurosci.*, vol. 13, no. 6, pp. 407–420, 2012.
- [4] E. J. D. Bronzino, "Neuman, M. R. 'Biopotential Electrodes.," Med. Instrum. Appl. Des., p. 713, 2010.
- [5] T. Yang, S. Hakimian, and T. H. Schwartz, "Intraoperative Electrocorticography(ECog): indications, techniques, and utility in epilepsy surgery," *Epileptic Disord.*, vol. 16, no. 3, pp. 271–279, 2014.
- [6] H. N. Schwerdt et al., "A Fully-Passive Wireless Microsystem for Recording of Neuropotentials using RF Backscattering Methods.," J. Microelectromechanical Syst., vol. 20, no. 5, pp. 1119–1130, 2011.
- [7] M. R. Neuman, "Biopotential amplifiers," Biomed. Eng. (NY)., no. 2, pp. 241–292, 2000.
- [8] F. Zhang, A. Mishra, A. G. Richardson, and B. Otis, "A low-power ECoG/EEG processing IC with integrated multiband energy extractor," *IEEE Trans. Circuits Syst. I Regul. Pap.*, vol. 58, no. 9, pp. 2069–2082, 2011.
- [9] H. M. Greiner et al., "Preresection intraoperative electrocorticography (ECoG) abnormalities predict seizure-onset zone and outcome in pediatric epilepsy surgery," Epilepsia, vol. 57, no. 4, pp. 582–589, 2016.
- [10] A. Yakovlev, S. Kim, and A. Poon, "Implantable biomedical devices: Wireless powering and communication," *IEEE Commun. Mag.*, vol. 50, no. 4, pp. 152–159, 2012.

- [11] C. W. L. Lee, A. Kiourti, and J. L. Volakis, "Miniaturized Fully Passive Brain Implant for Wireless Neuropotential Acquisition," *IEEE Antennas Wirel. Propag. Lett.*, vol. 16, pp. 645–648, 2017.
- [12] C. W. L. Lee, A. Kiourti, J. Chae, and J. L. Volakis, "A high-sensitivity fully passive neurosensing system for wireless brain signal monitoring," *IEEE Trans. Microw. Theory Tech.*, vol. 63, no. 6, pp. 2060–2068, 2015.
- [13] K. A. Psathas, A. Kiourti, and K. S. Nikita, "Biocompatibility of implantable antennas: Design and performance considerations," 8th Eur. Conf. Antennas Propagation, EuCAP 2014, no. EuCAP, pp. 1566–1570, 2014.
- [14] A. Kiourti, C. W. L. Lee, J. Chae, and J. L. Volakis, "A wireless fully passive neural recording device for unobtrusive neuropotential monitoring," *IEEE Trans. Biomed. Eng.*, vol. 63, no. 1, pp. 131–137, 2016.
- [15] B. Wodlinger, A. D. Degenhart, J. L. Collinger, E. C. Tyler-Kabara, and W. Wang, "The impact of electrode characteristics on electrocorticography (ECoG)," *Proc. Annu. Int. Conf. IEEE Eng. Med. Biol. Soc. EMBS*, vol. c, no. 1, pp. 3083–3086, 2011.
- [16] N. Van Camp, M. Verhoye, and a Van der Linden, "Stimulation of the rat somatosensory cortex at different frequencies and pulse widths.," *NMR Biomed.*, vol. 19, no. 1, pp. 10–17, 2006.
- [17] P. A. Valdés-Hernández, J. Bae, Y. Song, A. Sumiyoshi, E. Aubert-Vázquez, and J. J. Riera, "Validating Non-invasive EEG Source Imaging Using Optimal Electrode Configurations on a Representative Rat Head Model," *Brain Topogr.*, pp. 1–26, 2016.
- [18] G. Paxinos and C. Watson, The Rat Brain in Stereotaxic Coordinates, 6th ed. 2007.
- [19] A. Peyman et al., "The dielectric properties of biological tissues: I. Literature survey survey," 1996.
- [20] S. Gabriel, R. Lau, C. Gabriel, Gabriel S., Lau R.W., and Gabriel C., "The dielectric properties of biological tissues: II. Measurements in the frequency range 10 Hz to 20 GHz," *Phys. Med. Bioil.*, vol. 41, pp. 2251– 2269, 1996.
- [21] P. A. Valdés-Hernández, "An in vivo MRI Template Set for Morphometry, Tissue Segmentation, and fMRI Localization in Rats," Front. Neuroinform., vol. 5, no. November, pp. 1–19, 2011.